

# **Transient Flow in Porous Electrosprays**

Peter L. Wright<sup>1</sup> · Richard E. Wirz<sup>1</sup>

Received: 16 July 2022 / Accepted: 3 July 2024 © The Author(s), under exclusive licence to Springer Nature B.V. 2024

#### Abstract

Porous ionic electrospray emitters have received significant interest for space propulsion due to their performance and operational simplicity. We have developed a diffusion equation for describing the transient flow response in a porous electrospray emitter, which allows for the prediction of the settling time for flow in the porous emitter. This equation accounts for both the change in liquid storage at exposed pores on the emitter with pressure and viscous diffusion through Darcy's law. Transient flow solutions are provided for the most common emitter topologies: pillar, cone, and wedge. Transient flow solutions describe the settling time and magnitude of current overshoot from porous electrosprays, while providing useful guidelines for reducing transient response time through emitter design. Comparing diffusion of pressure to the onset delay model for electrospray emission shows that diffusion is most relevant at higher voltages and when a porous reservoir is used. Accounting for multiple emission sites on the wedge geometry shows that emission sites settle in proportion to emission site spacing to the power -1.74.

#### **Article Highlights**

- The transient response of porous electrosprays is affected by fluid storage in exposed pores.
- Pressure diffuses into a porous electrospray through depletion of fluid in exposed pores.
- Diffusion of pressure complements the existing onset delay model for porous electrosprays.

**Keywords** Electrospray · Porous media · Capillary action · Space propulsion

Published online: 18 July 2024

Mechanical and Aerospace Engineering, University of California Los Angeles, 420 Westwood Plaza, Los Angeles, CA 90095, USA



Peter L. Wright plloydwright@g.ucla.edu

### 1 Introduction

Electrospray emitters use a conductive liquid to produce an electrified meniscus from which charged droplets and/or ions are emitted. At the tip of the emitter, electrostatic stress and capillary pressure equilibrate to form a cone-like meniscus from which charged species emit. The three major categories of electrospray emitters (capillary, externally wetted, and porous) are distinguished by how propellant flows from the fluid reservoir to the emission surface. Of these, porous electrospray emitters have been of significant interest due to their simplicity and high performance.

In all applications of electrospray propulsion, dynamic events are unavoidable. When used for precision control, electrospray thrusters are continuously varied to provide the required thrust on a spacecraft (Demmons et al. 2019). Electrospray thrusters have also been operated under pulse-width-modulated (PWM) control, in which changes in the operating condition of the device are rapid and drastic (Courtney et al. 2018). Alternating polarity of emission is often implemented to increase device lifetime, which in turn can create a brief decrease in the applied electric field on the emission surface (Lozano and Martínez-Sánchez 2004). Each of these schemes results in time-dependent flow through the electrospray emitter. If the charge to mass ratio of emitted species has any dependence on flow to the emission sites, then time-dependent flow through the emitter can negatively affect the polydispersive efficiency, plume divergence, performance, and lifetime (Courtney et al. 2015; Wright et al. 2018; Thuppul et al. 2020). For these reasons, understanding the transient flow response of porous electrospray emitters is imperative to developing high-performance, long lifetime electrospray devices.

The objective of this effort is to develop mathematical expressions to describe the transient response of porous electrospray devices. The utility of predicting the transient response lies in the phenomenological description of transient settling and useful equations for reducing the transient settling time through informed emitter design. We have developed a fluid flow model for diffusion of pressure through a porous medium with exposed pores on nonemitting surfaces of the emitter. In Sect. 2 we will present the derivation of the governing equation for transient pressure diffusion in a porous medium from first principles. Then in Sect. 3 the governing equation will be applied to common porous electrospray emitter geometries. The presented theory is compared to the commonly used onset delay model in Sect. 5. Finally, the implications and challenges of the presented model are discussed in Sect. 6.

### 2 Theory

# 2.1 Steady-State Flow

In a porous electrospray emitter, propellant flows through the emitter substrate to the emission surface. The viscous loss associated with flow through a porous medium is described by Darcy's law:

$$\mathbf{u} = -\frac{k}{u}\nabla P,\tag{1}$$

where **u** is the fluid velocity, P is pressure, k is the porous permeability, and  $\mu$  is the fluid dynamic viscosity. This form of Darcy's law is valid for Reynolds number Re < 1, where inertial effects can be neglected (Bear 2013). The Reynolds number is described as Re =  $\rho ud/\mu$ , where  $\rho$  is the fluid density, and d is the particle size in the porous medium.



For boundary conditions, the reservoir pressure is the capillary pressure produced by a meniscus at a fully wetted pore upstream in the reservoir (Bear 2013; Hassanizadeh and Gray 1993) and the emission surface pressure is approximated by the Maxwell pressure supplied by the magnitude of the local primary extraction electric field,  $E_p$  (Smith 1986; Chen et al. 2006). The applied pressure difference from the fluid reservoir to emission site,  $\Delta P_{\rm app}$ , is:

$$\Delta P_{\rm app} = \frac{4\gamma}{D_{\rm res}} - \frac{1}{2}\epsilon_0 E_p^2,\tag{2}$$

where  $\gamma$  is the fluid surface tension coefficient,  $D_{\rm res}$  is the characteristic reservoir pore size, and  $\epsilon_0$  is the permittivity of free space. The electric field on the emitter surface has a linear relation to extraction voltage, which can be determined by computational simulation of the extraction geometry (Krpoun and Shea 2008; Wright and Wirz 2021) or through analytical evaluation of the extraction geometry (Smith 1986; Martinez-Sanchez and Lozano 2015). Equation 2 is undefined for cases where the electric pressure is less than the reservoir pressure, e.g., no electric field. For these cases, there is insufficient electric field to produce net flow from the reservoir through the emitter, so  $\Delta P_{\rm app} = 0$ .

#### 2.2 Transient Flow

In this section, expressions for the stored volume of fluid in each exposed pore will be combined with Darcy's law to develop a diffusion equation for pressure in a porous medium with exposed pores. As previously described, the flow within porous electrosprays is the result of decrease in pressure from the reservoir to the emission surface. Conservation of momentum in the streamwise direction shows how pressure gradient causes flow through the emitter. Perpendicular to the flow, pressure enforces the meniscus shape in exposed pores. As the meniscus changes, the amount of storable liquid in the pore changes as well. This phenomenon has been described diagrammatically by Lozano and Martinez-Sanchez (2005) for flow through grooves of externally wetted emitters and by Courtney and Shea (2015) for porous emitters. The fluid volume associated with the change in storable liquid at each pore must eventually pass through the emission surface downstream. In this way, exposed pores closest to the emission surface deplete as the flow settles to its steady-state condition. A diagram of flow through the porous emitter and the behavior of mensici with pressure is shown in Fig. 1.

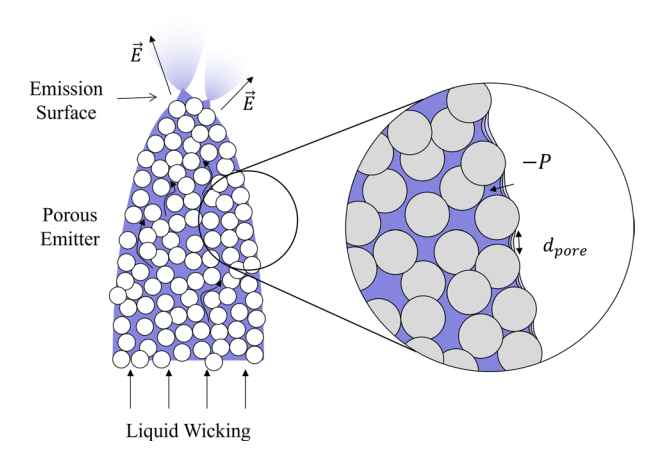
The curvature of the meniscus is found using the Young-Laplace equation, where the pressure drop across a meniscus,  $\Delta P_{\rm men}$ , is equal to the surface tension coefficient,  $\gamma$ , multiplied by the mean curvature of the meniscus. We assume that the meniscus forms a spherical shape, so the mean curvature is twice the reciprocal of the radius of the meniscus,  $R_{\rm men}$ :

$$\Delta P_{\rm men} = \frac{2\gamma}{R_{\rm men}}. (3)$$

We assume the device is operating in vacuum, i.e., there is no ambient pressure; the pressure drop across the meniscus can be replaced with the local pressure, *P*. For the case where there is no pressure difference across the meniscus, a flat surface is formed. As pressure decreases, the meniscus recedes into the porous medium and increases in curvature, resulting in a decreased capacity for storing liquid in the porous medium. The lost storage capacity of surface pores is determined as a spherical cap formed by the meniscus. For a



Fig. 1 Flow in a porous electrospray emitter, with a magnified cross section of a wetted porous surface. The meniscus of the liquid recedes into the porous medium as pressure decreases due to viscous dissipation



sufficiently smooth emitter surface, the bounds of the spherical meniscus are defined by the radius of a single-surface pore,  $R_{pore}$ . The volume of this spherical cap, V, and the depth that the meniscus has receded into its pore, h, are defined as:

$$V = \frac{1}{3}\pi h^2 (3R_{\text{men}} - h),\tag{4}$$

$$h = R_{\text{men}} \left( 1 - \left( 1 - \frac{R_{\text{pore}}^2}{R_{\text{men}}^2} \right)^{1/2} \right) \approx \frac{R_{\text{pore}}^2}{2R_{\text{men}}}.$$
 (5)

Equations 3 through 5 reveal the effect of local pressure on the pore's capacity for storing liquid,  $\Delta V_{\text{pore}}$ :

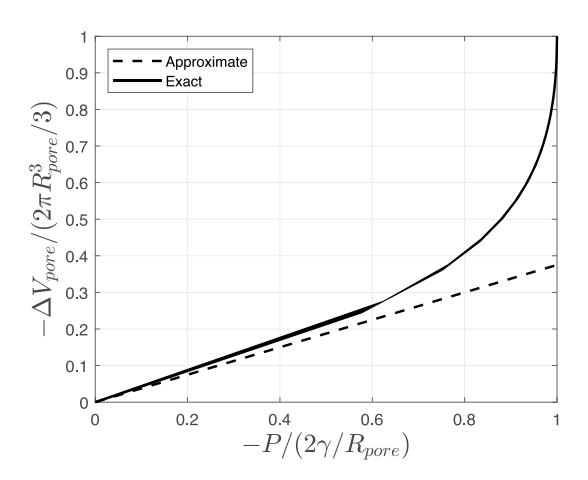
$$\Delta V_{\text{pore}} = \frac{\pi R_{\text{pore}}^4 P}{8\gamma}.$$
 (6)

The ability for a pore to store liquid is shown as a function of pressure is shown in Fig. 2, including the linearized form presented in Equation 6. The linearized relationship is 91% accurate within 50% of the characteristic pressure and 98% accurate within 25% of the characteristic pressure for saturated pores in the emitter porous medium  $(2\gamma/R_{pore})$  (Wright and Wirz 2021).

A common choice for porous medium is P5-grade porous glass, which has a pore radius of 0.5 to 0.8  $\mu$ m (Courtney and Shea 2015; Natisin et al. 2020; Ma et al. 2021). As an example, the emitter from Courtney and Shea (Courtney and Shea 2015) is considered, for which the electric field at the emission surface has been estimated as the emitter voltage multiplied by 15.3 mm<sup>-1</sup> (Wright and Wirz 2021). For EMI-BF4 in the emitter substrate, 5.7 kV is required to reach 25 % of the characteristic pressure of saturated porous in the emitter. The emitter was operated up to a maximum of 2.5 kV, which shows that the device was operated well within the range of validity for the linearization used to produce Equation 6. Even if the emitter was fabricated from P4-grade porous glass (as with Ma et al. 2021), which has a pore radius of 5 to 8  $\mu$ m, the operational range still falls within the 91% accuracy threshold for the linearization. For these



**Fig. 2** Volume of stored liquid in a pore as a function of pressure



reasons, we consider the linearization to be generally applicable to the common implementation of porous electrospray emitters. For pressures approaching the characteristic pressure of a pore, Equation 6 underestimates the change in volume with pressure, which both leads to underestimating transient settling time and loss of linearity with pressure.

The equation for continuity can be adjusted to account for the changing capacity for stored liquid volume in a differential element of known volume dV:

$$\nabla \cdot \mathbf{u} = -\frac{\partial}{\partial t} \frac{\Delta V}{dV}.\tag{7}$$

where t is time and  $\Delta V$  is the change in liquid capacity of an isobaric differential element due to the meniscus of exposed pores. The negative sign is adopted due to the convention in Eq. 6. Combined with Darcy's law, Eq. 7 becomes:

$$\frac{k}{\mu}\nabla^2 P = \frac{\partial}{\partial t} \frac{\Delta V}{\mathrm{d}V}.\tag{8}$$

Equation 8 is the governing equation for transient pressure in the porous domain that will be applied in this study, which states that the Laplacian of pressure is proportional to the change in the volume of liquid stored in a given differential element of the domain. Considering the change in stored liquid in the porous domain unfortunately causes Laplace's equation for pressure only to be valid when considering the steady-state response.

The nondimensional change in liquid capacity in a differential element,  $\Delta V/dV$ , can be expressed as a function of pressure through Eq. 6, the surface pore density  $n_{\text{pore}}$ , and the exposed surface area to volume ratio of a differential element:

$$\frac{\Delta V}{\mathrm{d}V} = \Delta V_{\mathrm{pore}} n_{\mathrm{pore}} \frac{dA}{dV} = \frac{\pi R_{\mathrm{pore}}^4 P}{8\gamma} \left(\frac{\epsilon}{\pi R_{\mathrm{pore}}^2}\right) \frac{\mathrm{d}A}{\mathrm{d}V}.$$
 (9)

where  $\epsilon$  is porosity. Equation 9 is used to convert Eq. 8 into a diffusion equation for pressure in a porous medium with an exposed surface, where D is the diffusion coefficient for this flow:



$$\frac{\partial}{\partial t}P = D\nabla^2 P; \quad D = \frac{8\gamma k}{\epsilon \mu R_{\text{pore}}^2} \frac{dV}{dA}.$$
 (10)

Diffusion equations have been previously derived to describe the evolution of pressure in porous media, relying upon properties such as fluid compressibility (Liang et al. 2001) or infiltration and pore deformation (Shapiro and Dinske 2009). Diffusion of pressure as presented in this section, and specifically in Eq. 10, is unique in its application and approach, but of course not the first to describe pressure diffusion in a porous medium. We justify the use of the term 'pressure diffusion' to describe the pressure response in the porous medium through the derivation of a diffusion governing equation to describe the process, specifically Eq. 10.

To estimate the diffusion coefficient for a porous emitter where the pore size and permeability are unknown, permeability is approximated through the Carman–Kozeny equation (Bear 2013) and pore size is approximated from particle size and porosity,  $\epsilon$ . If the porous medium has roughly circular pores between spherical particles, then:

$$R_{\text{pore}} = \frac{D_p}{2} \left( \frac{\epsilon}{1 - \epsilon} \right)^{1/2} \tag{11}$$

where  $D_p$  is the particle diameter. The diffusion coefficient can then be simplified as:

$$D = 0.178 \frac{\Phi^2 \gamma \epsilon}{\mu (1 - \epsilon)} \frac{dV}{dA}.$$
 (12)

where  $\Phi$  is a nondimensional parameter for particle sphericity (Kruczek 2014). Equation 12 shows that the diffusion coefficient can be reasonably estimated without performing pore size or permeability tests on a porous sample. Porosity can be measured from the mass of a porous sample with a known volume. The term  $\frac{dV}{dA}$  will depend on the geometry of the porous emitter. Regardless of geometry, pressure in the emitter domain settles over a timescale that is independent of change in pressure at the emission surface. As a result, the system response to a nondimensional pressure change at the emission surface can be characterized to understand the system response to any pressure change.

The description for pressure diffusion presented in this section is an analytical model and thus dependent on the accuracy of the assumptions and mathematical descriptions. Producing a porous medium is an inherently random process, which differs greatly from the uniform and isotropic porous media described in this section. Additionally, the accuracy of solutions to the diffusion equation proposed in Eq. 10 relies upon the accuracy of the chosen isobaric differential elements. With these limitations in mind, the presented model is best used for developing a phenomenological understanding of transient settling and informing emitter design to reduce the transient response, rather than to produce an exact prediction of the transient settling. The challenges and limitations of the pressure diffusion model will be further discussed in Sect. 6.

# 3 Modeling Common Electrospray Geometries

In this section, three common porous emitter geometries will be considered: pillar, cone, and wedge. For the cone and wedge geometries, example results are shown for the following conditions:  $R_I = 0.1$ ,  $R_O = 1$ ,  $D_O = 2$ , where  $R_I$  is the inner radius of the emission



surface,  $R_O$  is the radius of the base of the emitter, and  $D_0$  is a modified diffusion coefficient which has no spatial dependence. An instantaneous pressure jump from P=0 throughout the emitter domain to P=1 at the emission surface at time t=0 is considered to determine the transient response, regardless of emitter geometry. Full derivations of flow solutions are omitted for brevity; we refer the reader to Wright (2022) more detailed derivations.

## 3.1 Pillar Geometry

Pillar-shaped geometries are seldom used for porous electrospray emitters (Vasiljevich et al. 2008; Rojas-Herrera et al. 2017; Wright and Wirz 2021); however, the simplicity of the flow solution warrants analysis. The pillar emitter can be approximated as a semi-infinite cylinder. To determine the pressure response within the porous substrate, it is assumed to be at a uniform pressure before a disturbance is introduced at the tip of the semi-infinite domain at t = 0. The assumed geometry of the body and the differential element are shown in Fig. 3. Inside of the differential element, the fluid is assumed to be uniform pressure. The differential volume, dV, and differential surface area, dA, are determined from the thickness of the differential element, dy. The ratio of these two quantities is necessary for determining the diffusion coefficient.

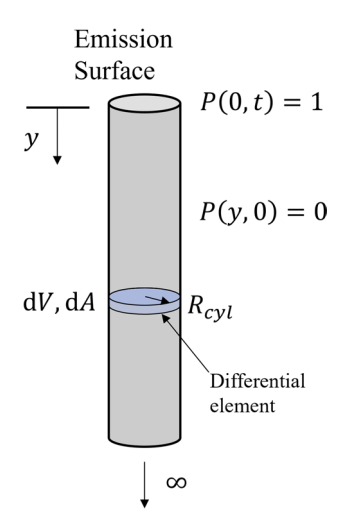
$$\frac{dV}{dA} = \frac{R_{\text{cyl}}}{2},\tag{13}$$

where  $R_{\rm cyl}$  is the radius of the cylinder. Thus the diffusion coefficient for a semi-infinite cylinder geometry per Eq. 10 is solved as:

$$D_{\rm cyl} = \frac{4\gamma k R_{\rm cyl}}{\epsilon \mu R_{\rm pore}^2}.$$
 (14)

Diffusion of a property such as pressure into a semi-infinite medium is often solved using a similarity solution (Panton 2013). For a nondimensionalized pressure disturbance upon the emission surface at t = 0 such that P(y, t = 0) = 0 and P(y = 0, t > 0) = 1, the solution for pressure is

Fig. 3 Geometry of a pillar emitter, with the differential element used in transient porous flow analysis specified





$$P = [1 - \text{erf}(\xi)]; \quad \xi = \frac{y}{2\sqrt{D_{\text{cyl}}t}},$$
 (15)

where  $\xi$  is a similarity variable. The pressure gradient at the tip is found by using the chain rule with Eq. 15 and the definition of the similarity variable  $\xi$ :

$$\frac{\partial P}{\partial y}(0,t) = \frac{1}{\sqrt{2\pi D_{\text{cyl}}t}}.$$
(16)

Flow rate through the emission surface decreases with time in proportion to the pressure gradient through Eq. 1. The similarity solution is no longer relevant when the pressure diffuses into the porous medium at a distance L from the emitter tip, thus forming the characteristic time,  $T_C$ , for this emitter geometry:

$$T_C = \frac{L^2}{4D} = \frac{L^2 \epsilon \mu R_{\text{pore}}^2}{16\gamma k R_{\text{cvl}}}.$$
 (17)

For  $t < T_C$ , flow is best described by the transient solution, while for  $t > T_C$ , the flow is best described by the steady flow solution. The flow response for a pillar-shaped emitter sheds light onto the characteristics of flow solutions obtained through the presented diffusion equation: flow through the emission surface decays nonlinearly and approaches the steady solution predicted through Darcy's law. This response also matches with the physical interpretation of the pressure diffusion into the porous medium, where fluid must be exhausted from exposed pores on the emitter surface before reaching an equilibrium state. Fluid accumulation in exposed pores temporarily reduces the effective hydraulic resistance of the emitter until excess fluid is exhausted through the emission surface. Additionally, note that while the fluid flow is toward the emission surface, pressure diffuses away from the emission surface as exposed pores exhaust accumulated fluid.

### 3.2 Cone Geometry

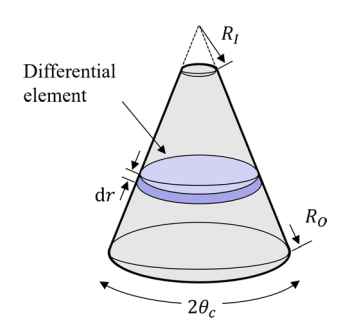
The cone geometry is the most widely adopted for use in porous electrospray emitters (Courtney et al. 2012; Ma et al. 2017; Liu et al. 2019; Natisin et al. 2020; Antypas and Wang 2019; Petro et al. 2020. A significant advantage of the cone shape compared to the wedge emitter is that the additional radius of curvature results in a sharper emitter tip, allowing for device operation at lower voltages. High emitter densities of 100 s of emitters per cm² have been implemented to achieve high-throughput density (Natisin and Zamora 2019; Huang et al. 2021a). When conventionally machined (Natisin et al. 2020) or electric discharge machined (Liu et al. 2019), the resulting emitter can be pyramid-shaped rather than cone-shaped; these two emitter shapes are sufficiently similar such that the two can be analyzed using the same flow geometry (Fig. 4).

The geometry for the cone emitter domain is shown in Fig. 4 with the chosen differential element. The diffusion coefficient for the cone geometry,  $D_c$ , is evaluated through element geometry and Eq. 10.

$$D_c = \frac{8\gamma kr}{\epsilon \mu R_{\text{pore}}^2} \left( 1 - \cos(\theta_c) \right) \cot(\theta_c) = D_{0,c} r.$$
 (18)



**Fig. 4** Left, geometry of a cone emitter, with the differential element used in transient porous flow analysis specified



For the cone geometry, the diffusion coefficient is no longer uniform over the domain of the emitter. For brevity, the diffusion coefficient for a cone,  $D_c$ , is replaced by  $D_{0,c}$ , which has no spatial dependence. To solve for the pressure response in the domain of the porous emitter, we consider a nondimensionalized pressure change at the emission surface at t = 0 such that P(r, t = 0) = 0 and  $P(R_I, t > 0) = 1$ . This transient heterogeneous problem is simplified as the superposition of steady solution,  $P_s$ , and homogeneous transient solution,  $P_t$  (Haberman 1983):

$$P(r,t) = P_s(r) + P_t(r,t).$$
 (19)

 $P_s$  satisfies boundary conditions  $P_s(R_O) = 0$ ,  $P_s(R_I) = 1$  and  $P_t$  satisfies homogeneous boundary conditions  $P_t(R_O, t) = P_t(R_I, t) = 0$ . The steady and homogeneous transient solutions combine to form the solution for nonhomogeneous boundary conditions at  $R_O$  and  $R_I$ . The steady-state solution for pressure in the cone,  $P_{c,s}$ , is found through Eq. 10, where time derivatives can be neglected:

$$P_{c,s}(r) = \frac{R_I}{R_O - R_I} \left( \frac{R_O}{r} - 1 \right). \tag{20}$$

A separation of variables solution is assumed in order to solve for the homogeneous transient component,  $P_{c,t}$ . Constant pressure boundary conditions are considered at the upstream and downstream boundaries, i.e.,  $P_{c,t}(R_O,t) = P_{c,t}(R_I,t) = 0$ . The homogeneous transient component of pressure in the domain is:

$$P_{c,t}(r,t) = \sum_{n=1}^{N} 2C_n \sqrt{\frac{D_0}{\lambda_n r}} e^{-\lambda_n t}$$

$$\times \left[ Y_1 \left( 2\sqrt{\frac{\lambda_n r}{D_0}} \right) - \frac{Y_1 \left( 2\sqrt{\frac{\lambda_n R_1}{D_0}} \right)}{J_1 \left( 2\sqrt{\frac{\lambda_n R_1}{D_0}} \right)} J_1 \left( 2\sqrt{\frac{\lambda_n r}{D_0}} \right) \right]$$
(21)

where  $J_1$  and  $Y_1$  are the Bessel functions of the first and second kind, respectively, both of order 1, and n refers to the nth value of  $\lambda$  that satisfies the boundary conditions, and N is the number of modes considered. Valid values of  $\lambda_n$  satisfy the boundary conditions through the following equation.



$$\frac{Y_1\left(2\sqrt{\frac{\lambda R_I}{D_0}}\right)}{J_1\left(2\sqrt{\frac{\lambda R_I}{D_0}}\right)} - \frac{Y_1\left(2\sqrt{\frac{\lambda R_O}{D_0}}\right)}{J_1\left(2\sqrt{\frac{\lambda R_O}{D_0}}\right)} = 0.$$
 (22)

The left-hand side of Eq. 22 is plotted in Fig. 5 with valid zeros.

The r-dependent terms in Eq. 21 are combined to find the bases for this equation  $R(\lambda_n, r)$ , shown in Fig. 5. Numerical projection of these bases onto each other shows that they are nonorthogonal, complicating the process for determining the proper values of  $C_n$  for approximating the steady solution. Coefficient values are determined by satisfying the initial condition P(r, t = 0) = 0 through Eq. 19. Values of  $C_n$  were determined through numerical optimization of the following equation, using seed values obtained through projecting  $P_{C,s}$  onto the basis functions:

$$P_{c,t}(r,t=0) = -P_{c,s}(r)$$
(23)

The success of this numerical optimization can be seen in the good agreement with the equilibrium solution through the basis functions, as shown in Fig. 5. The transient homogeneous solution captures the salient features of  $P_{c,t}$  with some periodic oscillation.

To obtain the heterogeneous transient solution, the equilibrium solution (Eq. 20) and homogeneous transient solution (Eq. 21) are added per Eq. 19. The solution can then be multiplied by the applied pressure difference, per Eq. 2.

### 3.3 Wedge Geometry

In this section, the wedge geometry of emitters will be considered. This geometry is less popular than the cone geometry, but has seen implementation in both research groups (Courtney and Shea 2015; Chen et al. 2020; Bretti 2020) and industry (Demmons et al. 2019). In contrast to cone-shaped emitters, wedge-shaped emitters have a linear extraction surface where the applied electric field is strong and ideally uniform. Numerous emission sites form on the emitter in this region, caused by electric field and hydraulic interactions (Courtney et al. 2019a; Wright and Wirz 2021). In contrast to cone emitters, these emitters will operate at

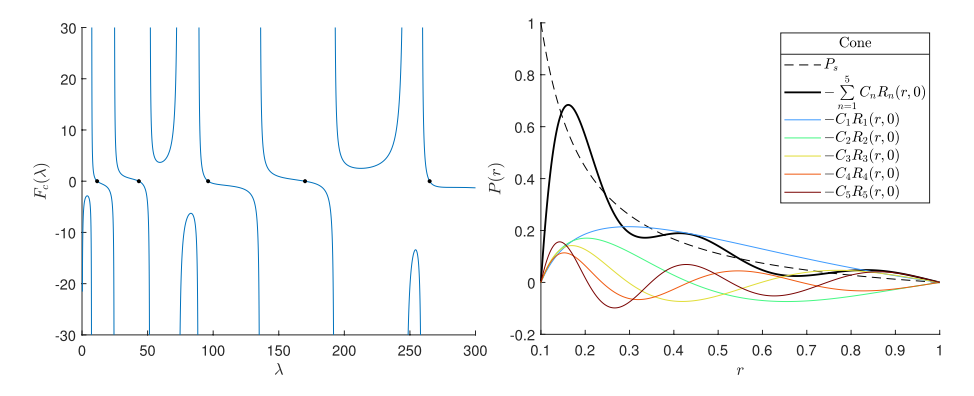


Fig. 5 Left, the left-hand side of Eq. 22, for  $R_I = 0.1$ ,  $R_O = 1$ , and  $D_{0,c} = 2$ , with valid zeros indicated. Right, the first 5 modes of the transient solution for the primary flow, with magnitudes determined through the described optimization strategy. The analytical approximation of the steady flow through these transient bases and the steady analytical solution are shown as well



a higher voltage due to only having one radius of curvature at the emission surface. On the other hand, only having curvature in one direction results in a narrow plume in the ridgewise direction of the wedge (Courtney et al. 2015; Liu et al. 2021). Additionally, the long-emission surface results in a tight collection of emission sites along the wedge without the need for emitter parallelization. For the wedge emitter, we consider flow in a cylindrical coordinate system. Because the governing equation is linear for this flow, the flow can be described by the superposition of a primary and secondary flow. The primary flow describes the net flow in the radial direction to the emission surface, while the secondary flow describes the local flow concentration to each emission site on the surface.

## 3.3.1 Primary Flow

The analytical geometry for flow in the wedge emitter domain is shown in Fig. 6. The diffusion coefficient from Eq. 10 is evaluated as:

$$D_{w} = \frac{4\gamma kr\theta}{\epsilon \mu R_{\text{pore}}^{2}} = D_{0,w}r,$$
(24)

As was the case for the cone emitter flow, the diffusion coefficient has an r-dependence, so  $D_w$  is replaced by  $D_{0,w}$  for brevity.

The steady solution,  $P_{w1,s}$  for  $P_{w1,s}(R_O) = 0$  and  $P_{w1,s}(R_I) = 1$  is:

$$P_{w1,s}(r) = \frac{\ln\left(\frac{R_O}{r}\right)}{\ln\left(\frac{R_O}{R_I}\right)}.$$
 (25)

Constant pressure boundary conditions are considered at the upstream and downstream boundaries, i.e.,  $P(R_O, t) = 0$  and  $P(R_I, t) = 0$ . To prevent a trivial solution,  $C_1$  is chosen such that  $R(R_O) = R(R_I) = 0$ . As with the cone flow, this yields a criterion for selecting values for  $\lambda$  that satisfy the boundary conditions of R:

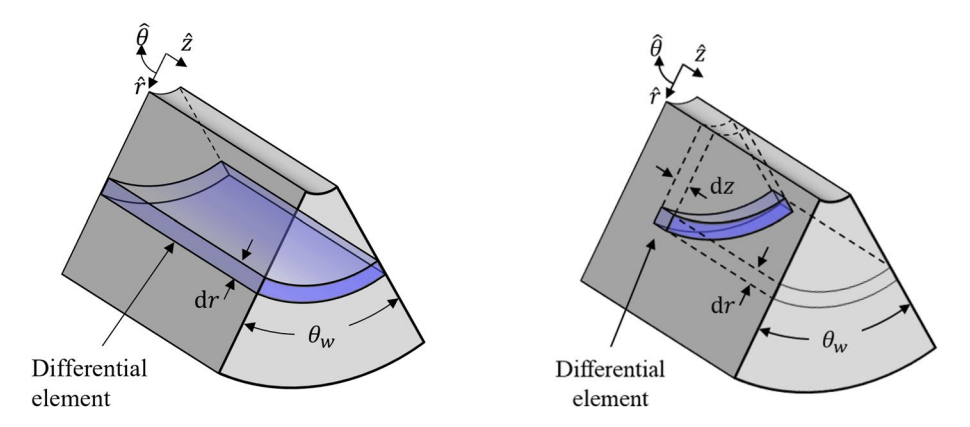


**Fig. 6** Geometry for flow in a wedge emitter. The differential elements used for analyzing the primary and secondary flows are shown in the subfigures at left and right, respectively

$$\frac{Y_0 \left(2\sqrt{\frac{\lambda_n R_I}{D_0}}\right)}{J_0 \left(2\sqrt{\frac{\lambda_n R_I}{D_0}}\right)} - \frac{Y_0 \left(2\sqrt{\frac{\lambda_n R_O}{D_0}}\right)}{J_0 \left(2\sqrt{\frac{\lambda_n R_O}{D_0}}\right)} = 0.$$
 (26)

For the wedge primary flow, the homogeneous transient solution has a form of:

$$P_{w1,t}(r,t) = \sum_{n=1}^{N} 2C_n \left[ Y_0 \left( 2\sqrt{\frac{\lambda_n r}{D_0}} \right) - \frac{Y_0 \left( 2\sqrt{\frac{\lambda_n R_t}{D_0}} \right)}{J_0 \left( 2\sqrt{\frac{\lambda_n R_t}{D_0}} \right)} J_0 \left( 2\sqrt{\frac{\lambda_n r}{D_0}} \right) \right] e^{-\lambda_n t}. \tag{27}$$

As with the solution for flow in the cone, the full solution is obtained by adding the transient homogeneous and steady solutions from Eqs. 27 and 25, respectively. The left-hand side of Eq. 26 and the bases of Eq. 27 are shown in Fig. 7.

# 3.3.2 Secondary Flow

The flow to individual emission sites is considered as the secondary flow. The governing equations for transient and steady flow are linear, so solutions can be superposed to form valid solutions. For the case where the base of the wedge,  $R_O$ , is much greater than the emission surface radius,  $R_I$ , and the emission site spacing,  $d_{\rm site}$ , Bessel I terms can be ignored in the steady solution (Wright and Wirz 2021). A sinusoidal pressure oscillation in z with an amplitude of 1 is assumed in order to develop an analytical approximation of the flow concentration into individual emission sites. The secondary flow can later be added to a matching primary flow from the previous section to enforce stagnation points in between each emission site.

For the transient secondary flow, the diffusion coefficient is the same as for the transient primary flow.

Assuming that the site spacing is smaller than  $R_O$ , the steady-state pressure in the domain,  $P_{w2.s}$ , is (Wright and Wirz 2021):

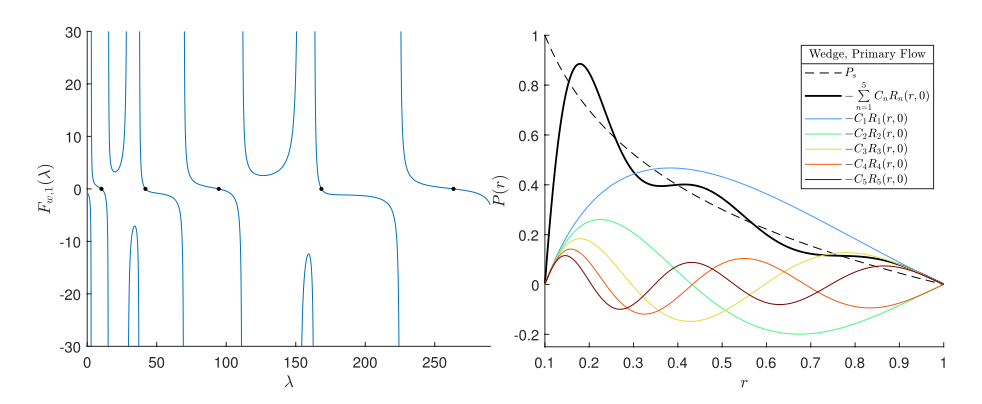


**Fig. 7** Left, the left-hand side of Eq. 26, for  $R_I = 0.1$ ,  $R_O = 1$ , and  $D_{0,w} = 2$ , with valid zeros indicated. Right, the first five modes of the transient solution for the primary flow, with magnitudes determined through projection of the steady flow solution. The analytical approximation of the steady flow through these transient bases and the steady analytical solution are shown as well



$$P_{w2,s}(r,z) = \frac{K_0(\alpha r)}{K_0(\alpha R_I)} e^{i\alpha z},$$
(28)

where  $\alpha$  is the wavenumber for the oscillating pressure condition at the emission surface and is equal to  $2\pi/d_{\text{site}}$ . A separation of variables approach was used to determine the transient pressure response in this domain:

$$P_{w2,t}(r,t,z) = \sum_{n=1}^{N} C_n e^{-\lambda_n t + \alpha(r - iz)} \times \left[ L_{\frac{1}{2} \left(\frac{\lambda_n}{D_0 \alpha} - 1\right)}(2\alpha r) - \frac{U\left(\frac{1}{2} - \frac{\lambda_n}{2D_0 \alpha}, 1, 2\alpha r\right)}{U\left(\frac{1}{2} - \frac{\lambda_n}{2D_0 \alpha}, 1, 2\alpha R_I\right)} L_{\frac{1}{2} \left(\frac{\lambda_n}{D_0 \alpha} - 1\right)}(2\alpha R_I) \right]$$
(29)

where U is the confluent hypergeometric function of the second kind (Weisstein 2003a) and L is the Laguerre polynomial (Weisstein 2003b). Values of  $\lambda$  satisfy the following equation:

$$\frac{U\left(\frac{1}{2} - \frac{\lambda_n}{2D_0\alpha}, 1, 2\alpha R_I\right)}{L_{\frac{1}{2}\left(\frac{\lambda_n}{D_0\alpha} - 1\right)}(2\alpha R_I)} - \frac{U\left(\frac{1}{2} - \frac{\lambda_n}{2D_0\alpha}, 1, 2\alpha R_O\right)}{L_{\frac{1}{2}\left(\frac{\lambda_n}{D_0\alpha} - 1\right)}(2\alpha R_O)} = 0.$$
(30)

Satisfying Eq. 30 appears to be a necessary but not sufficient criterion; valid flow solutions with values for  $\lambda$  that satisfied Eq. 30 were determined through inspection. Valid solutions for  $\lambda$  are shown in Fig. 8 with their associated bases from Eq. 29.

The added complexity due to inclusion of an additional independent flow parameter motivates simplification of the transient behavior prediction. As with the other flows discussed previously, the long-term behavior of the flow is described by the first eigenvalue, while higher eigenvalues describe successively shorter-term behavior. Understanding the first eigenvalue allows for understanding the envelope of transient settling for the flow. The secondary flow in a porous wedge is largely confined to the emission surface; as long as

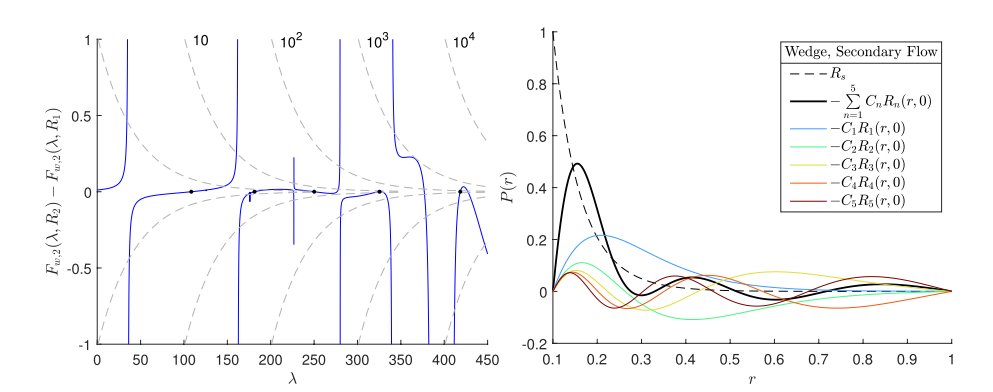


Fig. 8 Left, the left-hand side of Eq. 30, for  $R_I = 0.1$ ,  $R_O = 1$ ,  $D_{0,w} = 2$ , and  $d_{\rm site} = 0.5$ , with valid zeros indicated. Note that a variable scale for the vertical axis is utilized to highlight interesting features of Eq. 30. Right, the first 5 modes of the transient solution for the secondary flow, with magnitudes determined through the described optimization strategy. The analytical approximation of the steady flow through these transient bases and the steady analytical solution are shown as well



 $R_I$  and  $d_{\rm site}$  are significantly smaller than the base of the wedge  $R_O$ , the base radius  $R_O$  has negligible effect on the secondary flow. Approximate values for the first eigenvalue can be found by neglecting the second term in Eq. 30 through the argument that the flow is confined to the emission surface. Dimensional analysis suggests a solution of the form:

$$\lambda_1 \propto \frac{D_{0,w} R_I^m}{d_{vite}^{m+1}} \equiv \eta, \tag{31}$$

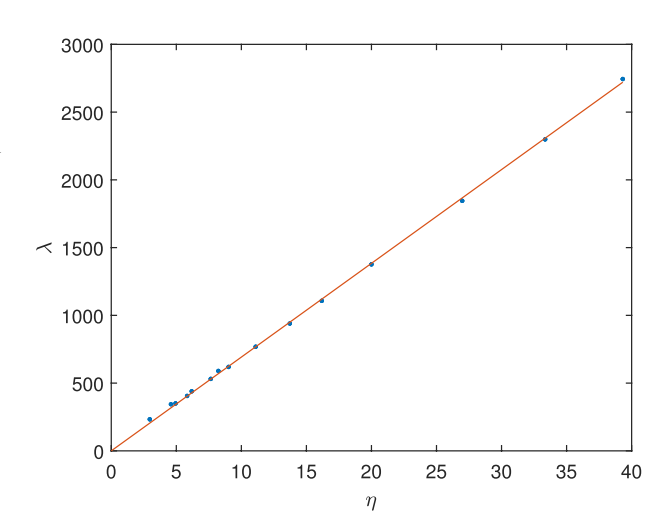
where  $\eta$  is a nondimensional parameter capturing the combined effect of  $d_{\text{site}}$  and  $R_I$  on  $\lambda$ . Least squares fitting over a range of input parameters suggests a proportionality coefficient of 69.2 and m = 0.738. The first eigenvalue of the wedge secondary flow for a variety of geometric parameters is shown in Fig. 9.

Because the secondary flow is confined to the region of the emitter near the emission surface, the time required for this flow to settle will generally be much shorter than that of the primary flow. When considering large changes to the pressure condition at the emission surface of an electrospray, the secondary flow settling should be considered when a detailed understanding of the transient response is required. However, emission sites can be unsteady even at a constant operating condition (Juraschek and Röllgen 1998). For capillary emitters, oscillations in the cone are coupled with the unsteadiness of the jet on the order of single kHz frequencies (Choi et al. 2008); in porous electrosprays, the porous medium may act as another mechanism for unsteady emission with lower frequencies possible as a function of emission site spacing. Equation 31 predicts that settling time increases with site spacing to the power -1.738. In other words, higher frequency pulsating emission sites are expected when emitting with high emission site densities.

## 4 Error Estimation

The analytical results from Sect. 3 are supported by a numerical solver, which uses the finite difference method with an explicit time step to predict the temporal response of pressure in the medium. The time step was chosen to ensure a Von Neumann stability

Fig. 9 The first eigenvalue of the wedge secondary flow for  $D_{0,w} = 2$  and values of  $R_I$  from 0.1 to 0.25,  $R_I$  from 5 to 10, and  $d_{site}$  from 0.1 to 0.3. Dimensional analysis and least squares fitting show good agreement with the numerically determined zeros with fit parameters of A = 69.2 and m = 0.738 per Eq. 31





parameter of less than 0.2 throughout the domain (Kajishima and Taira 2016). The error of each analytical solution,  $\sigma$ , is estimated by comparing the analytical flow field to that which was produced by the numerical solver, normalized by the pressure integrated over the domain:

$$\sigma(t) = \frac{\sqrt{\sum_{x=1}^{X} (P_d(x,t) - P_a(x,t))^2}}{\sum_{x=1}^{X} P_d(x,t)},$$
(32)

where  $P_d$  is the pressure obtained by the discretized method,  $P_a$  is the pressure obtained by analytical the analytical solution for the specified emitter geometry, x is the location from the discretized solver, and X is the number of points used in the discretized solver. Equation 32 was used to evaluate the accuracy of the analytical expressions for the transient pressure response of the cone, primary wedge, and secondary wedge flows.

The error in the transient pressure solutions for the cone and wedge domains is shown in Figs. 10, 11, and 12. Error decreases over time and with an increase in the number of evaluated modes. Due to the nonorthogonality of modes in the cone flow, increasing the number of modes does not necessarily decrease error over the entire time domain. For the secondary wedge flow, error is initially high and decreases sharply around  $1/\lambda_N$ . Analytical modes produce pressure oscillation throughout the spatial domain of the emitter, while the physical response is mostly confined to within  $d_{\rm site}$  from  $R_I$ , resulting in initially high error.

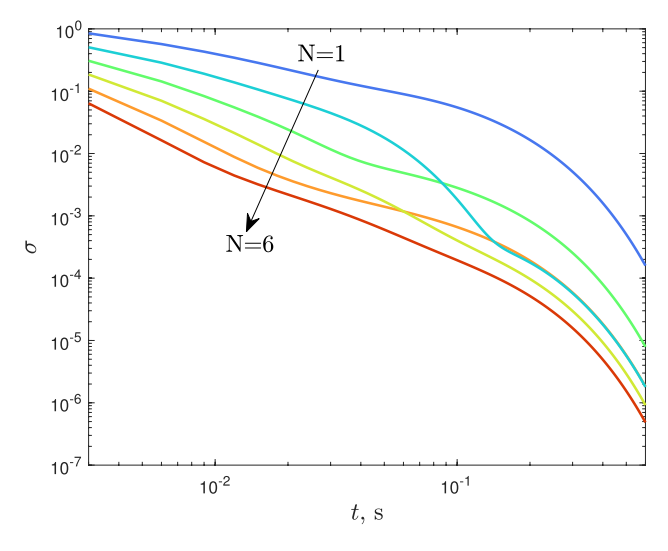


Fig. 10 Error associated with analytical approximation of the transient flow in a porous cone, using up to the first six modes in Eq. 21



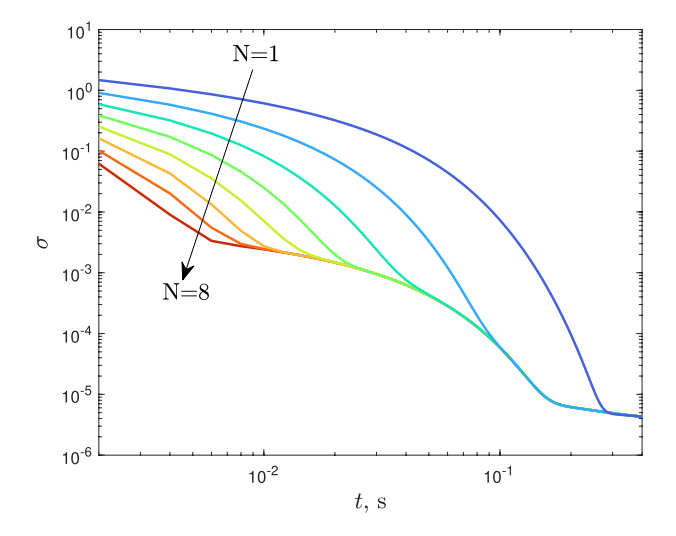
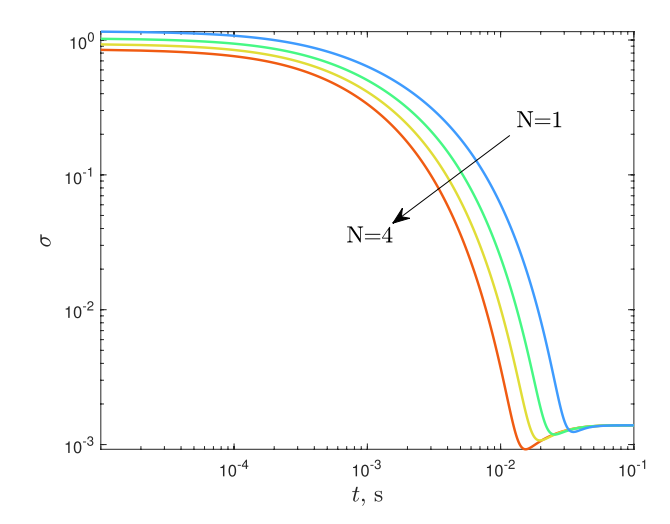


Fig. 11 Error associated with analytical approximation of the transient primary flow in a porous wedge, using up to the first eight modes in Eq. 27

Fig. 12 Error associated with analytical approximation of the transient secondary flow in a porous wedge, using up to the first four modes in Eq. 29



# 5 Comparison with Onset Delay Evaluation

A commonly used method of evaluating the time response of an electrospray is through onset delay characterization. Thompson and Prowett developed the onset delay model by considering viscous effects and the volume associated with a Taylor cone during emission (Thompson and Prewett 1984). The theory has been applied to experimental results from externally wetted electrosprays (Lozano and Martínez-Sánchez 2005) and porous electrosprays using Darcy's law to understand the effect of viscosity (Huang et al. 2021b).

Onset delay and diffusion of pressure, as presented in this study, are complementary models because the first describes only up to the time of emission, while the latter is



more suited to understanding the flow once emission is underway. On the other hand, they are similar models in that the flow can be considered settled once a sufficient volume of fluid has passed through the emitter. By comparing the propellant volume throughput required to reach steady state, the two models can be compared to see when each are relevant. For simplicity, the presented pressure diffusion is evaluated for a cylindrical, or pillar style, emitter.

To determine the onset delay, the volume of a Taylor cone at the emission surface must be evaluated. While an ideal Taylor cone takes an angle of 49.3° due to the balance of surface tension and electric pressure, fluid pressure can cause the shape to differ from this ideal geometry. When using a porous reservoir, fluid can be supplied to the emission sites at a strong negative pressure, causing a smaller Taylor cone with a concave cross section. This phenomenon is supported by empirical evidence (Mair 1997) and analytical models (de La Mora 2007; Coffman 2016; Coffman et al. 2019).

The volume of a Taylor cone with a strong restorative pressure is considered by assuming an ideal Taylor shape, but reducing the radius of the base of the emission site in response to the negative fluid pressure in the porous medium. The radius of the meniscus at the base is determined by finding the size at which the restorative pressure, electric pressure, and surface tension effects are comparable. This assumption results in the onset cone volume shrinking with restorative pressure, which is consistent with experimental measurements of cone volume decreasing with voltage (Huang et al. 2021b) and onset voltage increasing with restorative pressure (Courtney and Shea 2015). Analytical modeling predicts that the radius of the base of the cone scales with  $\gamma/P_{\rm res}$  (de La Mora 2007). The surface tension pressure is assumed to be equal to that of the restorative pressure at the analytical approximation for the base of the cone:

$$P_{\rm res} = \frac{\gamma}{R_{\nu}} = \frac{4\gamma}{D_{\rm res}},\tag{33}$$

where  $D_{\rm res}$  is the pore diameter of the porous reservoir and  $R_{\gamma}$  is a characteristic radius of the emission site at onset. We assume that there is one emission site at startup, generally the number of emission sites at startup is of order 1 (Peter et al. 2020; Krejci et al. 2017). The volume of a cone,  $V_{\rm TC}$ , can be determined from its base radius,  $R_{\rm TC}$ , and height,  $h_{\rm TC}$ :

$$V_{\text{TC}} = \frac{1}{3}\pi R_{\text{TC}}^2 h_{\text{TC}} = \frac{1}{3}\pi \left( R_{\gamma} \cos(\theta_{\text{TC}}) \right)^2 \frac{R_{\gamma} \cos^2(\theta_{\text{TC}})}{\sin(\theta_{\text{TC}})},\tag{34}$$

$$V_{\rm TC} = \frac{\pi D_{\rm res}^3 \cos^4(\theta_{\rm TC})}{192 \sin(\theta_{\rm TC})} \approx 0.0039 D_{\rm res}^3,$$
 (35)

where  $\theta_{TC}$  is the ideal Taylor cone half angle of 49.3 °. As previously discussed, the expression for cone volume shown in Eq. 35 is an approximation that is informed by experimental and analytical results. The approach presented above assumes that the capillary pressure plays the most significant role during onset, which contrasts with other models that assume cone size is a result of pore size (Whittaker et al. 2022) or sintered particle size (Ober et al. 2010). For a given porous electrospray emitter, the three interpretations can lead to nearly an order of magnitude spread in the estimated cone size (Wright 2022). Due to the various models for cone volume, Eq. 35 is better used for evaluating phenomenological trends than for precise predictions.



For the effect of pressure diffusion through the porous emitter, the change in volume can be evaluated by comparing the change in propellant volume from the initial condition to the steady-state emission condition. At startup, the pressure throughout the emitter is uniformly at the reservoir pressure. The stored liquid associated with diffusion of pressure,  $V_{\rm diff}$ , is evaluated over the surface of the emitter:

$$V_{\text{Diff}} = \int \Delta V_{\text{pore}} n_{\text{pore}} dS = \frac{\pi \epsilon R_{\text{pore}}^2 RL}{8\gamma} \left( \frac{1}{2} \epsilon_0 E^2 - \frac{4\gamma}{D_{\text{res}}} \right), \tag{36}$$

where the electric field imposed on the emission surface depends on the applied voltage difference and geometry of the porous emitter. Note that while it is tempting to estimate the settling time by combining the stored liquid volume per Eq. 36 and the steady-state flow rate from the steady-state pressure profile per Eq. 20, this method may not produce an accurate estimate of settling time. The steady-state flow rate is at best a crude estimate of the time-averaged transient flow rate.

To determine whether a given emitter is expected to operate in an onset delay dominated mode or a diffusion dominated mode, a ratio of the two propellant volumes,  $\hat{V}$ , is formed by dividing Eq. 35 by Eq. 36:

$$\hat{V} = \frac{V_{\text{TC}}}{V_{\text{Diff}}} = \frac{\gamma D_{\text{res}}^3 \cos^4(\theta_{\text{TC}})}{24\epsilon R_{\text{pore}}^2 RL \sin(\theta_{\text{TC}})} \left(\frac{1}{2}\epsilon_0 E^2 - \frac{4\gamma}{D_{\text{res}}}\right)^{-1}.$$
 (37)

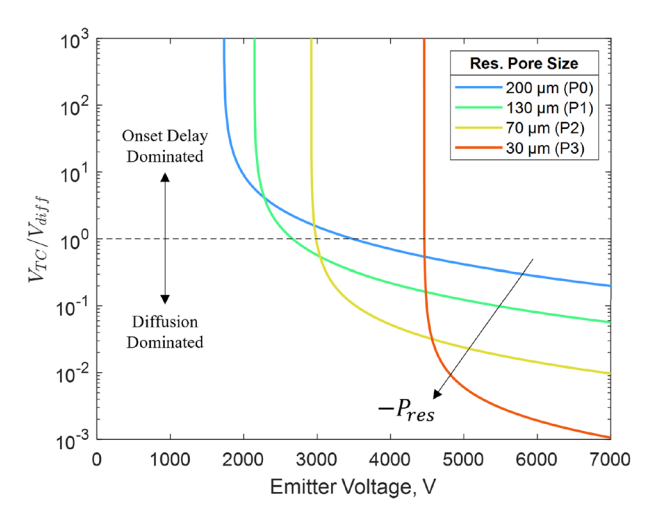
Large values of  $\hat{V}$  (i.e.,  $\hat{V}\gg 1$ ) indicate that much more propellant is stored in the Taylor cone at startup than will be wicked from surface pores away from the emission surface. More specifically, available propellant will be wicked away from surface pores before filling the Taylor cone volume required for startup. For this case, it is expected that onset delay will dominate the transient response of such an emitter. On the other hand, small values for  $\hat{V}$  indicate that the volume of a Taylor cone at startup will be filled well before available propellant in emitter surface pores has been depleted. For this case, it is expected that pressure diffusion will dominate the transient response.

Equation 37 is plotted in Fig. 13 for a pillar emitter with various porous reservoirs, EMI-Im as a working fluid, and emitter geometry and material properties per Wright and Wirz (2021):  $\gamma = 0.038 \text{ Nm}^{-1}$ , R = 0.5 mm, L = 5 mm,  $C_E = 7.8 \text{ mm}^{-1}$ ,  $\epsilon = 0.23$ , and  $R_{\text{pore}} = 1.5 \text{ \mu m}$ . From this plot, four major observations are noted.

Firstly, onset delay is expected to dominate the transient behavior of an emitter near its startup voltage. For electrospray devices operating at emission voltages, Eq. 35 predicts large Taylor cone size, while the volume associated with porous diffusion is small. Secondly, increasing the applied voltage is expected to cause the transient behavior to be more dominated by diffusion. The volume throughput associated with diffusion of pressure increases with voltage, while the volume in a Taylor cone decreases. Thirdly, increasing the restorative pressure, as shown by decreasing reservoir pore size from P0 to P3, causes diffusion to dominate the transient emitter response. The restorative pressure associated with small pore-size reservoirs is expected to have a strong effect on reducing the size of Taylor cones near startup. Finally,  $\hat{V}$  spans multiple orders of magnitude for the range of variables considered, showing that the conclusions are relevant given the accuracy described for Eq. 35. These observations are supported by empirical evidence of onset delay dominating the transient response for porous electrospray emitters used without a porous reservoir (Huang et al. 2021b) and negligible onset delay for electrospray emitters using a porous reservoir (Courtney et al. 2019b).



Fig. 13 Comparing the volume required to fill a Taylor cone on the emission surface to the fluid volume stored in surface pores of the emitter as a function of emitter voltage and reservoir porosity grade. The transient response of a porous emitter is predicted to be dominated by onset delay if this volume ratio is large, or dominated by pressure diffusion if this volume is small



This is not to say that pressure diffusion is a replacement for onset delay models when characterizing the transient response of porous electrospray emitters, but rather that there are regimes where one or the other dominate the transient response. Both perspectives are important for characterizing the transient response of electrospray emitters.

### 6 Discussion

In this section, we aim to discuss and review the behavior of electrospray devices as related to the transient flow model presented in this manuscript. Additionally, the model has limitations in its applicability and challenges that reduce its accuracy.

The six key conclusions regarding transient settling in porous emitters are as follows:

- The settling time can be reduced through informed emitter design, either through Eq. 17 or by finding the first root of Eqs. 22, 26, or 30. Increasing the diffusion coefficient and decreasing the height of emitters will lead to shorter settling times. Surface tension and permeability decrease the transient settling time, while porosity, viscosity, and pore size increase settling time. Generally, short-and-wide geometries are advantageous for decreasing settling time.
- Diffusion of pressure causes exponential decay in emission in response to voltage changes. Initially the response will be steeper-than-exponential decay due to the superposition of short- and long-wavelength modes. For the latter half of the emission response, short-wavelength modes will have decayed and the half-wavelength mode will dominate the emission response.
- Onset delay dominates the emitter response near the startup voltage. Operating at
  higher voltages increases the applied pressure difference on the emitter, increasing
  the flow through the emitter. Because the diffusion of pressure is linear, the settling
  time is expected to be independent of emitter voltage. As a result, diffusion of pressure
  becomes more important at higher voltages.
- Onset delay becomes negligible with increasing restorative pressure. As reservoir pore size decreases, the Taylor cone volume is expected to decrease, with the settling time



- for diffusion of pressure again remaining constant. Diffusion becomes more important as smaller pore reservoirs are incorporated into the emitter assembly.
- Emission sites settle more quickly as they densify. As the site density increases, the
  region of the emitter influenced by the secondary flow to each emission site decreases,
  which in turn decreases the settling time. Pulsating emission sites are expected to
  increase in frequency with proximity to adjacent emission sites.
- The settling time can be approximated even if the details of the porous medium are
  unknown. If the porous medium is formed from a homogeneous mixture of sintered
  spherical particles, the porous permeability can be estimated through the CarmanKozeny equation. The permeability scales with the square of particle size, while pore
  size is proportional to particle size, so the particle size has negligible effect on the diffusion coefficient.

This analysis describes the settling of flow in a porous medium, but does not investigate the flow within the Taylor cone. For a complete picture of the transient response of an electrospray emitter, it will be important to develop a deeper understanding of how the electric field manifests as a pressure well at each emission site. Coupling the emission site behavior with pressure and flow rate at the base of the Taylor cone is necessary to develop a complete understanding of the transient emission behavior. Furthermore, the quantitative comparison of pressure diffusion and onset delay models is hindered by the analytical representation of the volume required for an emission site at onset. An analytical or empirical model describing the onset volume as a function of operational conditions would be valuable for quantitative comparison of the two identified transient emission models.

The model is limited by how well the differential elements represent constant pressure surfaces. Although the analysis assumes that the isobaric surfaces are constant-y surfaces for the pillar emitter or constant-r surfaces for the cone emitter and wedge primary flow, in reality these surfaces will bulge upstream. The additional flow associated with transient settling originates from fluid volume stored in surface pores, so streamlines will be deflected toward the emitter centerline or centerplane, while these pores deplete. Once the flow settles, flux from nonemitting surfaces associated with pore depletion vanishes and the constant potential surfaces match the differential elements for the transient flow. Because constant pressure surfaces approach the differential element geometry over time, the elements can be considered to reasonably approximate the flow. For a more accurate representation of transient settling, an additional direction of flow would need to be considered for each of the presented geometries (e.g., flow in the r- and  $\theta-$ directions for the wedge primary flow) and the domain would need to be split into interior elements where Darcy's law is enforced and exterior elements where Eq. 10 is enforced. Such an approach would lead to an improvement in the accuracy of analytical predictions of transient settling to the detriment of the simplicity of analytical relations produced by the effort, such as Eq. 26.

The menisci formed at the surface of the emitter are assumed to be constrained by single pores. However, if the manufacturing process results in a rough emitter surface, this assumption may not hold. For example, conventional machining of glass occasionally produces visible chips in the emitter between the scale of the emitter and sintered particle (Natisin and Zamora 2019; Antypas and Wang 2019). If the roughness is of a scale less than the reservoir pore size, then menisci on the emitter surface may span multiple pores. In this case, the assumptions used to develop Eq. 4 may not hold, resulting in an underestimate of fluid stored in exposed pores and thus of transient settling time. As a result, the presented diffusion equation presented in this manuscript is most applicable to emitters with smooth nonemitting surfaces.



While this study has focused on pressure diffusion within the emitter structure of an electrospray device, the entire flow system should be considered for a more comprehensive understanding of transient device behavior. For example, pooling may occur between emitter structures when an open or pressurized reservoir is used (Chen et al. 2020), which may violate the assumptions used to derive Equation 6 or provide alternative flow paths. Although a porous reservoir can be used to introduce a Laplace pressure (Courtney and Shea 2015), which should prevent pooling, it introduces additional porous flow elements. Extending the presented analysis to further upstream elements, such as the porous reservoir, is suggested for future research. Transient settling has been observed over the scale of minutes and hours during device operation (Courtney et al. 2018); depletion of pores in the porous reservoir is suggested as a potential pathway to understanding long-scale flow settling behavior.

#### 7 Conclusion

In conclusion, a diffusion equation for pressure in porous electrospray devices has been developed from first principles for capillary action and porous flow. The diffusion equation has been applied to common emitter geometries and compared to the onset delay model for electrospray emission, showing how emitter design and operation affect which regime best describes the transient response of a porous emitter. As electrosprays are considered for more ambitious missions, the effects of transient flow on device lifetime, minimum impulse bit, and thrust noise spectra become more important to understand. We encourage future researchers to consider characterizing their porous materials and transient response in order to understand this feature of electrospray emitter operation.

Acknowledgements Thank you to David Ren and Jean Marques Helder Ribeiro for helpful discussions.

### **Declarations**

**Funding** This work was supported by NASA Space Technology Research Fellowship grant #80NSSC18K1194. The authors have no relevant financial or nonfinancial interests to disclose.

#### References

Antypas, R.J., Wang, J.J.: Pure ionic electrospray extractor design optimization. In: International Electric Propulsion Conference, p. 372. ERPS (2019)

Bear, J.: Dynamics of Fluids in Porous Media. Courier Corporation, North Chelmsford (2013)

Bretti, M.: Ais-ilis1 ionic liquid ion source electrospray thruster. Appl. Ion Syst. LLC (2020)

Chen, C., Chen, M., Zhou, H.: Characterization of an ionic liquid electrospray thruster with a porous ceramic emitter. Plasma Sci. Technol. (2020)

Chen, C., Saville, D., Aksay, I.A.: Scaling laws for pulsed electrohydrodynamic drop formation. Appl. Phys. Lett. **89**(12), 124103 (2006)

Choi, H.K., Park, J.-U., Park, O.O., Ferreira, P.M., Georgiadis, J.G., Rogers, J.A.: Scaling laws for jet pulsations associated with high-resolution electrohydrodynamic printing. Appl. Phys. Lett. 92(12), 123109 (2008)

Coffman, C., Martínez-Sánchez, M., Higuera, F., Lozano, P.C.: Structure of the menisci of leaky dielectric liquids during electrically-assisted evaporation of ions. Appl. Phys. Lett. 109, 231602 (2016)

Coffman, C.S., Martínez-Sánchez, M., Lozano, P.C.: Electrohydrodynamics of an ionic liquid meniscus during evaporation of ions in a regime of high electric field. Phys. Rev. E 99, 063108 (2019)



- Courtney, D.G., Alvarez, N., Demmons, N.R.: Electrospray thrusters for small spacecraft control: Pulsed and steady state operation. In: Joint Propulsion Conference, p. 4654. AIAA (2018)
- Courtney, D.G., Dandavino, S., Shea, H.: Comparing direct and indirect thrust measurements from passively fed ionic electrospray thrusters. J. Propuls. Power **32**(2), 392–407 (2015)
- Courtney, D.G., Li, H.Q., Lozano, P.: Emission measurements from planar arrays of porous ionic liquid ion sources. J. Phys. D: Appl. Phys. 45, 485203 (2012)
- Courtney, D.G., Shea, H.: Influences of porous reservoir Laplace pressure on emissions from passively fed ionic liquid electrospray sources. Appl. Phys. Lett. 107, 103504 (2015)
- Courtney, D.G., Wood, Z., Fedkiw, T.: Reconstructing electrospray plume current spatial distributions using computed tomography. In: International Electric Propulsion Conference, p. 787. ERPS (2019)
- Courtney, D.G., Wood, Z., Gray, S., Model, J. High-speed transient characterization of the Busek bet-300-p electrospray thruster. In: 2019 International Electric Propulsion Conference (2019)
- de La Mora, J.F.: The fluid dynamics of Taylor Cones. Annu. Rev. Fluid Mech. 39, 217–243 (2007)
- Demmons, N.R., Wood, Z., Alvarez, N. Characterization of a high thrust, pressure-fed electrospray thruster for precision attitude control applications. Propulsion and Energy Forum, p. 3817. AIAA (2019)
- Haberman, R.: Elementary Applied Partial Differential Equations, vol. 987. Prentice Hall, Englewood Cliffs (1983)
- Hassanizadeh, S.M., Gray, W.G.: Thermodynamic basis of capillary pressure in porous media. Water Resour. Res. **29**(10), 3389–3405 (1993)
- Huang, C., Li, J., Li, M.: Performance measurement and evaluation of an ionic liquid electrospray thruster. Chin. J. Aeronaut. (2021)
- Huang, C., Li, J., Li, M., Si, T., Xiong, C., Fan, W.: Experimental investigation on current modes of ionic liquid electrospray from a coned porous emitter. Acta Astronaut. 183, 286–299 (2021)
- Juraschek, R., Röllgen, F.: Pulsation phenomena during electrospray ionization. Int. J. Mass Spectrom. 177, 11–15 (1998)
- Kajishima, T., Taira, K.: Computational Fluid Dynamics: Incompressible Turbulent Flows. Springer, Berlin (2016)
- Krejci, D., Mier-Hicks, F., Thomas, R., Haag, T., Lozano, P.: Emission characteristics of passively fed electrospray microthrusters with propellant reservoirs. J. Spacecr. Rockets 54(2), 447–458 (2017)
- Krpoun, R., Shea, H.R.: A method to determine the onset voltage of single and arrays of electrospray emitters. J. Appl. Phys. **104**(6), 064511 (2008)
- Kruczek, B.: Carman-Kozeny equation. Encyclopedia of membranes, pp. 1-3 (2014)
- Liang, Y., Price, J.D., Wark, D.A., Watson, E.B.: Nonlinear pressure diffusion in a porous medium: Approximate solutions with applications to permeability measurements using transient pulse decay method. J. Geophys. Res. Solid Earth 106(B1), 529–535 (2001)
- Liu, X., He, W., Kang, X., Xu, M.: Fabrication of porous emitters for ionic liquid ion source by wire electrical discharge machining combined with electrochemical etching. Rev. Sci. Instrum. 90(12), 123304 (2019)
- Liu, X., Kang, X., Deng, H., Sun, Y.: Energy properties and spatial plume profile of ionic liquid ion sources based on an array of porous metal strips. Plasma Sci. Technol. 23, 12 (2021)
- Lozano, P., Martínez-Sánchez, M.: Ionic liquid ion sources: suppression of electrochemical reactions using voltage alternation. J. Colloid Interface Sci. 280(1), 149–154 (2004)
- Lozano, P., Martínez-Sánchez, M.: On the dynamic response of externally wetted ionic liquid ion sources. J. Phys. D Appl. Phys. **38**(14), 2371 (2005)
- Ma, C., Bull, T., Ryan, C.: Feasibility study of a micro-electrospray thruster based on a porous glass emitter substrate. In: International Electric Propulsion Conference, p. 485. ERPS (2017)
- Ma, C., Bull, T., Ryan, C.N.: Plume composition measurements of a high-emission-density electrospray thruster. J. Propuls. Power 37(6), 816–831 (2021)
- Mair, G.: The effects of flow impedance on the current-voltage characteristics of liquid-metal ion sources. J. Phys. D Appl. Phys. 30(13), 1945 (1997)
- Martinez-Sanchez, M., Lozano, P.: 16.522 Space Propulsion. MIT OpenCourseWare (2015)
- Natisin, M., Zamora, H., McGehee, W., Arnold, N., Holley, Z., Holmes, M., Eckhardt, D.: Fabrication and characterization of a fully conventionally machined, high-performance porous-media electrospray thruster. J. Micromech. Microeng. **30**(11), 115021 (2020)
- Natisin, M.R., Zamora, H.L.: Performance of a fully conventionally machined liquid-ion electrospray thruster operated in PIR. In: International Electric Propulsion Conference, p. 522. ERPS (2019)
- Ober, S., Branam, R., Huffman, R., Demmons, N., Martin, R.: Electrospray thruster for cubesat. In: 49th AIAA Aerospace Sciences Meeting Including the New Horizons Forum and Aerospace Exposition, p. 522 (2010)
- Panton, R.L.: Incompressible Flow. Wiley, Hoboken (2013)



- Peter, B.S., Dressler, R.A., Chiu, Y.-H., Fedkiw, T.: Electrospray propulsion engineering toolkit (ESPET). Aerospace 7(7), 91 (2020)
- Petro, E., Bruno, A., Lozano, P., Perna, L.E., Freeman, D.: Characterization of the TILE electrospray emitters. AIAA Propulsion and Energy 2020 Forum, p. 3612
- Rojas-Herrera, J., Jivanescu, I., Freeman, D., Krejci, D., Fucetola, C., Lozano, P.: Porous materials for ionelectrospray spacecraft microengines. J. Nanomech. Micromech. 7(3), 04017006 (2017)
- Shapiro, S.A., Dinske, C.: Fluid-induced seismicity: pressure diffusion and hydraulic fracturing. Geophys. Prospect. 57(2), 301–310 (2009)
- Smith, D.P.: The electrohydrodynamic atomization of liquids. IEEE Trans. Ind. Appl. IA-22, 3527–535 (1986)
- Thompson, S., Prewett, P.: The dynamics of liquid metal ion sources. J. Phys. D Appl. Phys. 17(11), 2305 (1984)
- Thuppul, A., Wright, P.L., Collins, A.L., Ziemer, J.K., Wirz, R.E.: Lifetime considerations and estimation for electrospray thrusters. Aerospace 78, 108 (2020)
- Vasiljevich, I., Tajmar, M., Grienauer, W., Plesescu, F., Buldrini, N., Gonzalez del Amo, J., ... Betto, M.: Development of an indium mn-feep thruster. In: 44th aiaa/asme/sae/asee Joint Propulsion Conference and Exhibit, p. 4534 (2008)
- Weisstein, E.W.: . Confluent hypergeometric function of the second kind. From MathWorld–A Wolfram Web Resource. https://mathworld.wolfram.com/ConfluentHypergeometricFunctionoftheSecondKind. html (2003a)
- Weisstein, E.W.: Laguerre polynomial. From MathWorld—A Wolfram Web Resource. https://mathworld.wolfram.com/LaguerrePolynomial.html (2003b)
- Whittaker, C.B., Eckels, J., Gorodetsky, A.A., Jorns, B.A.: A moment-based model of multi-site emission for porous electrosprays. In: 37th International Electric Propulsion Conference (2022)
- Wright, P., Thuppul, A., Wirz, R.E.: Life-limiting emission modes for electrospray thrusters. In: 2018 Joint Propulsion Conference p. 4726 (2018)
- Wright, P., Wirz, R.E.: Transient flow in porous electrospray emitters. AIAA Propulsion and Energy 2021 Forum, p. 3437 (2021)
- Wright, P.L.: Porous Electrospray Fluid Mechanics. University of California, Los Angeles (2022)
- Wright, P.L., Wirz, R.E.: Multiplexed electrospray emission on a porous wedge. Phys. Fluids 33, 012003 (2021)

**Publisher's Note** Springer Nature remains neutral with regard to jurisdictional claims in published maps and institutional affiliations.

Springer Nature or its licensor (e.g. a society or other partner) holds exclusive rights to this article under a publishing agreement with the author(s) or other rightsholder(s); author self-archiving of the accepted manuscript version of this article is solely governed by the terms of such publishing agreement and applicable law.

